Appl. Phys. B 80, 321–328 (2005)
DOI: 10.1007/s00340-004-1716-y

Applied Physics B
Lasers and Optics

F.-B. XIONG[1,2]
Z.-D. LUO[1]
Y.-D. HUANG[1,✉]

Spectroscopic properties of Pr^{3+} in anisotropic $PbWO_4$ crystal

[1] Fujian Institute of Research on the Structure of Matter, Chinese Academy of Sciences, Fuzhou, Fujian 350002, P.R. China
[2] Graduate School of the Chinese Academy of Sciences, Beijing 100039, P.R. China

Received: 15 September 2004/
Revised version: 2 November 2004
Published online: 21 December 2004 • **© Springer-Verlag 2004**

ABSTRACT The polarized absorption spectra, polarized fluorescence spectra, and fluorescence decay curves of Pr^{3+} ions in anisotropic $PbWO_4$ single crystal, which was grown by the modified Bridgman method, were measured at room temperature. The standard and modified Judd–Ofelt theories, extended to anisotropic crystal, have been applied to analyze the spectra. The spectroscopic parameters, including the Judd–Ofelt intensity parameters Ω_t ($t = 2, 4, 6$), spontaneous emission probabilities, fluorescence branching ratios, radiative lifetimes, stimulated emission cross sections, and fluorescence quantum efficiencies, were estimated. The good spectroscopic properties show the possible application of the Pr^{3+}-doped $PbWO_4$ crystal as solid-state and self-stimulated Raman laser materials.

PACS 78.20.-e; 42.70.Hj

1 Introduction

Lead tungstate crystal $PbWO_4$, known as scintillating crystal because of its high density, short radiation length, and fast decay time, has been widely investigated [1]. Recently, the Raman spectra of the $PbWO_4$ crystal and stimulated Raman laser action of this crystal pumped by Q-switched Nd^{3+}:YAG have been reported [2], in which beyond 50% total efficiency of Stokes conversion has been achieved. Furthermore, much attention has been paid to the crystal as promising solid-state and self-stimulated Raman laser hosts [3–5]. The pulsed and continuous-wave fundamental laser emissions from the Nd^{3+}-doped $PbWO_4$ crystal have been realized [4]. A passively Q-switched, self-stimulated Raman laser with about 56% optical frequency-conversion efficiency has also been realized in a laser diode pumped Nd^{3+}:$PbWO_4$/Cr^{4+}:YAG system [5].

The Pr^{3+} ion has an intricate energy-level scheme with an energy gap of various magnitudes and a rich emission spectrum extending from the ultraviolet (UV), visible, to near-infrared (NIR) regions. So, the Pr^{3+}-doped materials are attractive in optical fiber amplifiers [6], quantum cuttings [7], up-conversion lasers [8], and tunable UV and vacuum UV solid-state lasers [9].

✉ Fax: +86-591-8371-4946, E-mail: huyd@fjirsm.ac.cn

The optical spectra of Pr^{3+}:$PbWO_4$ at 90 K have been interpreted within the framework of the crystal-field theory, and the crystal-field parameters and the Stark levels have been calculated [10]. On the other hand, the influence of Pr^{3+} or other lanthanum doping ions on the scintillation characteristics of $PbWO_4$ has been studied [11, 12], and the influence of oxygen vacancies and Pr^{3+} impurity ions on the scintillation properties of $PbWO_4$ has been investigated on the basis of the electronic structure calculations [13]. However, to our knowledge, the detailed spectroscopic properties of this crystal as solid-state and self-stimulated Raman laser materials have not been analyzed until now. Especially, $PbWO_4$ is a uniaxial crystal and belongs to the tetragonal system with space group of $C_{4h}^6 - I4_1/a$ [2]. It is well known that there are considerable differences between polarized and non-polarized spectra for anisotropic crystal, so the analysis of polarized spectra is necessary for the evaluation of laser properties of Pr^{3+}:$PbWO_4$ crystal.

In this work, based on the polarized spectra recorded at room temperature and the Judd–Ofelt (J–O) theory [14, 15], the spectroscopic parameters of Pr^{3+} in $PbWO_4$ crystal are calculated and the laser properties of the Pr^{3+}:$PbWO_4$ crystal are evaluated.

2 Experimental procedure

$PbWO_4$ single crystal doped with Pr^{3+} ions was grown by the modified Bridgman method in the State Key Laboratory of High Performance Ceramics and Superfine Microstructure (Shanghai, China). The growth procedure is similar to that of Nd^{3+}:$PbWO_4$ described in [3]. The density of the crystal is 8.23 g/cm^3 [2]. The sample used in the spectral experiments was cut from the grown crystal with dimensions of $1.56 \times 0.79 \times 0.21$ cm^3 and the c axis is perpendicular to the face of 1.56×0.21 cm^2. All the surfaces of the sample were polished.

The concentration of Pr^{3+} ions in the sample was measured to be 1.67×10^{20} cm^{-3} (1.53 at. %) by inductively coupled plasma atomic emission spectrometry (ICP-AES, IRIS Advantage, THERMO-JARRELL ASH).

The polarized spectra and fluorescence decay curves were measured at room temperature. The absorption spectra were recorded using a spectrophotometer (Lambda900, Perkin-Elmer) with a spectral range from 340 to 2700 nm. When

the sample was excited at 449, 590, and 1030 nm and transited to the $^3P_2$, $^1D_2$, and $^1G_4$ manifolds, respectively, the polarized fluorescence spectra in ranges of 470 to 1080 nm, 620 to 1500 nm, and 1250 to 1450 nm were recorded using a spectrophotometer (FL920, Edinburgh), respectively. In the measurements, the fluorescence signals were collected at 90° from the excitation beam and focused on the entrance slit of the monochromator. Polarization of the fluorescence was selected by placing a prism polarizer between the focusing lens and the entrance slit of the monochromator. To calibrate the spectral responses of the detector and monochromator for different polarizations, the sample was firstly oriented with the c axis parallel to the optical path of detection; by keeping the sample and excitation beam fixed and rotating the polarizer, the fluorescence spectra with vertical and horizontal polarizations were recorded. Due to both of them being the σ–($E\perp c$) polarized spectra, the emission intensities are equal at any wavelength and the two spectra with vertical and horizontal polarizations can be used to calibrate the spectral responses of the detector and monochromator for different polarizations. Then the crystal was oriented with the c axis perpendicular to the optical path of detection and the σ–($E\perp c$) and π–($E//c$) polarized fluorescence spectra were recorded and calibrated using the method mentioned above. The responses of the monochromator and detector at different wavelengths were also corrected using a standard lamp (calibrated in the National Institute of Metrology, Beijing, China). The spectral resolutions of both the absorption and the fluorescence spectra were 1.0 nm. The fluorescence decay curves at 490 and 706 nm, corresponding to the $^3P_0 \rightarrow {}^3H_4$ and $^1D_2 \rightarrow {}^3H_5$ transitions, were recorded using a spectrophotometer (FL920, Edinburgh). A nanosecond flash lamp (nF900, Edinburgh) with pulse width of about 1.6 ns at 449 nm was used to excite the Pr^{3+} ions to the $^3P_2$ manifold and then populate the $^3P_0$ manifold quickly by non-radiative relaxation; the fluorescence signals of the $^3P_0 \rightarrow {}^3H_4$ transition were detected with a photomultiplier tube (PMT, R955, Hamamatsu). A microsecond flash lamp (μF900, Edinburgh) with pulse width of about 1 μs at 590 nm was used as the excitation source for the $^1D_2 \rightarrow {}^3H_5$ transition; the signals were detected with a NIR PMT (R5509, Hamamatsu). Due to the lack of an appropriate excitation source, the measurement of the fluorescence decay curve from the $^1G_4$ manifold was not performed.

The ordinary and extraordinary refractive indices of $PbWO_4$ crystal in a range from 375 to 700 nm were provided in [16]. By fitting these data, a rough Sellmeier equation of the refractive indices was obtained:

$$n_o^2 = 4.724 + \frac{0.087}{\lambda^2 - 0.073}\,, \tag{1}$$

$$n_e^2 = 4.522 + \frac{0.052}{\lambda^2 - 0.071}\,. \tag{2}$$

In the following spectral analysis, the values of ordinary and extraordinary refractive indices of $PbWO_4$ crystal were used for σ–($E\perp c$) and π–($E//c$) polarized spectra, respectively.

3 Results and discussion

3.1 *Absorption spectra*

The room-temperature σ- and π-polarized absorption spectra for Pr^{3+}:$PbWO_4$ crystal are shown in Fig. 1. The base lines in the spectra, which are caused by the reflection of the crystal surface and the defects in the crystal, have been corrected. The absorption bands correspond to the transitions from ground manifold $^3H_4$ to various excited manifolds. It can be seen from the figure that the absorption coefficients of the π-polarized spectrum are larger than those of the σ-polarized spectrum except for the absorption peaks around 1500 nm, corresponding to the $^3H_4 \rightarrow {}^3F_3 + {}^3F_4$ transitions. It is worth noting that there are some high-absorption peaks between 440 and 500 nm in both σ- and π-polarized absorption spectra, so that the Pr^{3+}:$PbWO_4$ crystal can be effectively pumped by visible sources, such as an argon-ion laser and a blue diode laser.

3.2 *Judd–Ofelt analysis*

The J–O theory [14, 15] is the most effective method in the analysis of spectroscopic properties of rare-earth ions in crystals and glasses. By means of the calculation of the J–O intensity parameters Ω_t ($t = 2, 4, 6$) from the absorption spectra, the spontaneous emission probability, fluorescence branching ratio, and radiative lifetime of excited manifold can be estimated.

For Pr^{3+} ions, the magnetic dipolar contributions to the absorption and emission line strengths are very weak [17], so the magnetic dipole transitions have not been taken into account in the J–O calculation of the ions. The absorption line strength of a transition from ground manifold $^3H_4$ ($J = 4$) to an excited J' manifold, $S_{\mathrm{mea}}(J \rightarrow J')$, can be obtained from the corresponding absorption spectral band measured at room temperature by [18]

$$S_{\mathrm{mea}}\left(J \rightarrow J'\right) = \frac{3hc\,(2J+1)}{8\pi^3 e^2 \bar{\lambda}_{\mathrm{abs}} N_0} \frac{9n}{\left(n^2+2\right)^2} \Gamma\,, \tag{3}$$

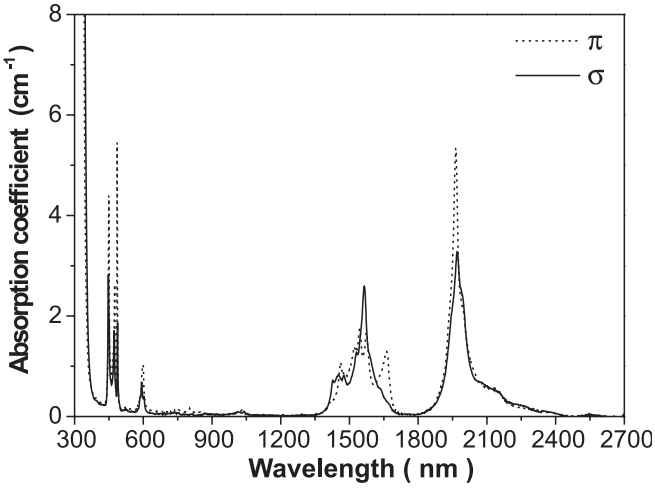

FIGURE 1 Room-temperature polarized absorption spectra of Pr^{3+}:$PbWO_4$ crystal

where N_0 is the Pr^{3+} concentration expressed in ion/cm^3, $\bar{\lambda}_{abs}$ is the mean wavelength of the absorption band, n is the refractive index of the sample, c is the velocity of light, e is the charge of an electron, and Γ is the integrated absorption coefficient for the absorption band and is expressed as

$$\Gamma = \int_{J \to J'} \alpha(\lambda)\, \mathrm{d}\lambda\,, \tag{4}$$

where $\alpha(\lambda)$ is the measured absorption coefficient as a function of wavelength λ. In Fig. 1, seven bands can be distinguished from the absorption spectra. It must be pointed out that when absorption bands of transitions from the ground manifold to several excited manifolds overlap seriously and display as one band in the spectra, the total integrated absorption coefficient of the band is treated as one experimental datum. The values of the measured line strengths of Pr^{3+}:$PbWO_4$ are listed in Table 1. According to the J–O theory, the absorption line strength can also be expressed in terms of the parameters Ω_t ($t = 2, 4, 6$) as

$$S_{\mathrm{cal}}\left(J \to J'\right) = \sum_{t=2,4,6} \Omega_t \left|\left\langle 4f^n\,[\alpha SL]\, J \left\| U^{(t)} \right\| 4f^n\left[\alpha' S' L'\right] J'\right\rangle\right|^2, \tag{5}$$

where the reduced unit tensor matrix elements $\left\langle 4f^n\,[\alpha SL]\, J \left\| U^{(t)} \right\| 4f^n\left[\alpha' S' L'\right] J'\right\rangle^2$ are approximately independent of the host crystal and the values of the elements can be found from [19, 20]. Just as in [19–21], an intermediate-coupling approximation is adopted and the wave function $|4f^n\,[\alpha SL]\, J\rangle$ is a linear combination of the Russell–Saunders states $|4f^n \alpha SLJ\rangle$. For the bands including more than two absorption transitions, the sums of the corresponding matrix elements were used. By a least-square fitting between (3) and (5), the J–O parameters Ω_t ($t = 2, 4, 6$) for σ and π polarizations could be obtained from the σ- and π-polarized absorption spectra, respectively. The root mean square (RMS) deviation between the experimental and calculated line strengths is defined as

$$\mathrm{RMS}\ \Delta S = \sqrt{\frac{\sum_{i=1}^{N} (S_{\mathrm{mea}} - S_{\mathrm{cal}})^2}{N-3}}\,, \tag{6}$$

where N is the number of experimental bands taken into account in the above calculation. The relative error is defined as

$$\mathrm{RMS\ error} = \frac{\mathrm{RMS}\ \Delta S}{\mathrm{RMS}\ S} \times 100\%\,, \tag{7}$$

where

$$\mathrm{RMS}\ \ S = \sqrt{\frac{\sum_{i=1}^{N} S_{\mathrm{mea}}^2}{N}}\,.$$

The values of the J–O parameters Ω_t ($t = 2, 4, 6$), RMS ΔS and RMS error are listed in Table 2.

In the calculation of the J–O parameters, the difficulty found by many authors in the Pr^{3+} ions [22, 23], i.e. an unphysical negative value for the parameter Ω_2, was not encountered for the Pr^{3+}:$PbWO_4$ crystal.

As in most cases [22, 24, 25], the J–O parameters have also been calculated while the hypersensitive $^3H_4 \to {}^3P_2$ transition is excluded in the fitting procedure. In Table 2, the values of the parameters are listed and compared with those including the $^3H_4 \to {}^3P_2$ transition. The two sets of J–O parameters do not have a large discrepancy, but the values of RMS ΔS decrease from 1.17×10^{-20} cm^2 (σ) and 0.95×10^{-20} cm^2 (π) to 1.00×10^{-20} cm^2 (σ) and 0.51×10^{-20} cm^2 (π), respectively, and the values of RMS error decrease from 23.1% (σ) and 16.6% (π) to 18.5% (σ) and 8.3% (π), respectively.

There are several modified methods for obtaining the J–O parameters [26–28] of Pr^{3+} ions. In [27], the disagreement between the calculated and experimental results was attributed to the low-lying $4f5d$ state in Pr^{3+} ions, which makes the probabilities of transitions from ground manifold to high-lying manifolds in the $4f^2$ configuration more than those calculated by the standard J–O theory. So, a modified J–O theory has been introduced to take the effect of the lowest

Transition	σ-polarized $S(J \to J')(10^{-20}$ cm$^2)$			π-polarized $S(J \to J')\ (10^{-20}$ cm$^2)$		
$^3H_4 \to$	$\bar{\lambda}_{abs}$(nm)	S_{mea}	S_{cal}	$\bar{\lambda}_{abs}$(nm)	S_{mea}	S_{cal}
$^3P_2$	449	2.38	-	450	2.88	-
$^3P_1$	472	1.33	1.38	473	1.44	1.88
$^1P_0$	488	0.91	0.84	486	1.63	1.21
$^1D_2$	593	0.88	0.77	596	1.33	0.72
$^1G_4$	1025	0.22	0.11	1030	0.22	0.13
$^3F_3 + {}^3F_4$	1554	8.89	8.89	1554	9.67	9.66
$^3F_2 + {}^3H_6$	1986	9.56	9.56	1983	11.08	11.10

TABLE 1 Mean wavelengths and measured and calculated line strengths of polarized absorption spectra for Pr^{3+}:$PbWO_4$ crystal at room temperature (a *dash* indicates that the datum is not available)

	The standard J–O theory				The modified J–O theory			
	$^3H_4 \to {}^3P_2$ included		$^3H_4 \to {}^3P_2$ excluded		$^3H_4 \to {}^3P_2$ included		$^3H_4 \to {}^3P_2$ excluded	
	σ	π	σ	π	σ	π	σ	π
Ω_2	8.20	11.19	8.40	13.25	18.78	21.17	18.94	21.39
Ω_4	10.49	9.99	10.40	7.12	4.79	6.93	4.85	7.01
Ω_6	3.16	3.99	3.04	4.83	7.56	7.64	7.31	7.29
RMS ΔS	1.17	0.95	1.00	0.51	0.57	0.88	0.10	0.49
RMS error (%)	23.1	16.6	18.5	8.3	11.3	15.3	1.9	8.1

TABLE 2 J–O parameters of Pr^{3+}:$PbWO_4$ crystal determined by different approaches and the corresponding root mean square deviations RMS ΔS and RMS error (Ω_t ($t = 2, 4, 6$) and RMS ΔS are in units of 10^{-20} cm^2)

$4f5d$ state into account; the absorption line strength is rewritten as [27]

$$S_{\mathrm{cal}}\left(J \to J'\right) = \sum_{t=2,4,6} \Omega_t \left|\left\langle 4f^n\,[\alpha SL]\,J \left\| U^{(t)} \right\| 4f^n\left[\alpha' S' L'\right] J'\right\rangle\right|^2 \times \left[1 + \left(E_J + E_{J'} - 2E_f^0\right)\Big/\left(E_{5d} - E_f^0\right)\right], \quad (8)$$

where E_J, $E_{J'}$, and E_{5d} are the energies of the initial manifold, final manifold, and the lowest $4f5d$ state, respectively, E_f^0 is the average energy of all the optically accessible $4f^2$ states, and other parameters have the same meaning as in (5).

This modified J–O theory was also used in this work to calculate the J–O parameters and the values of E_{5d} and E_f^0, $60\,000\,\mathrm{cm}^{-1}$ and $10\,000\,\mathrm{cm}^{-1}$, respectively, were taken from [28]. Both calculations with and without the ${}^3H_4 \to {}^3P_2$ transition were made. All the results are also listed and compared in Table 2. It reveals that the modified J–O theory without the ${}^3H_4 \to {}^3P_2$ transition gives the best fitting results for the absorption line strengths. The values of RMS ΔS are $0.10 \times 10^{-20}\,\mathrm{cm}^2$ (σ) and $0.49 \times 10^{-20}\,\mathrm{cm}^2$ (π), respectively, and the values of RMS error are 1.9% (σ) and 8.1% (π), respectively. In the following analysis, the parameters Ω_t ($t = 2, 4, 6$) determined by the modified J–O theory without the ${}^3H_4 \to {}^3P_2$ transition are adopted.

The calculated absorption line strengths are also listed in Table 1. Luo et al. [29] have proposed that for anisotropic crystal the corresponding effective J–O parameters should be $\Omega^{\mathrm{eff}} = (2\Omega_\sigma + \Omega_\pi)/3$. So, the effective J–O parameters of Pr^{3+}:$PbWO_4$ crystal are $\Omega_2^{\mathrm{eff}} = 19.76 \times 10^{-20}\,\mathrm{cm}^2$, $\Omega_4^{\mathrm{eff}} = 5.57 \times 10^{-20}\,\mathrm{cm}^2$, and $\Omega_6^{\mathrm{eff}} = 7.30 \times 10^{-20}\,\mathrm{cm}^2$.

3.3 *Radiative transitions*

The spontaneous emission probability for a transition from an excited manifold J to a lower manifold J', $A_{JJ'}$, can be calculated by

$$A_{JJ'}\left(J \to J'\right) = \frac{64\pi^4 e^2}{3h\,(2J+1)\,\bar{\lambda}_{\mathrm{em}}^3} \frac{n\left(n^2+2\right)^2}{9} \times \sum_{t=2,4,6} \Omega_t \left\langle 4f^n\,[\alpha SL]\,J \left\| U^{(t)} \right\| 4f^n\left[\alpha' S' L'\right] J'\right\rangle^2 \times \left[1 + \left(E_J + E_{J'} - 2E_f^0\right)\Big/\left(E_{5d} - E_f^0\right)\right], \quad (9)$$

where $\bar{\lambda}_{\mathrm{em}}$ is the mean wavelength of the emission band and the values of $U^{(t)}$ ($t = 2, 4, 6$) have been proposed by Kaminskii [19, 20]. Then, the fluorescence branching ratios for the excited manifold can be determined by

$$\beta = \frac{A_{JJ'}\left(J \to J'\right)}{\sum_{J'} A_{JJ'}\left(J \to J'\right)}. \quad (10)$$

For anisotropic crystal, the total spontaneous emission probability should be $A_{\mathrm{total}}\left(J \to J'\right) = \left(2A_{\mathrm{total}}^{\sigma} + A_{\mathrm{total}}^{\pi}\right)/3$, and the radiative lifetime τ_{r} of manifold J is expressed as

$$\tau_{\mathrm{r}} = \frac{1}{\sum_{J'} A_{\mathrm{total}}\left(J \to J'\right)}. \quad (11)$$

Transition	$\bar{\lambda}_{\mathrm{em}}$(nm)	π-polarized $A_{JJ'}(\mathrm{s}^{-1})$	π-polarized β(%)	σ-polarized $A_{JJ'}(\mathrm{s}^{-1})$	σ-polarized β(%)	τ_r(μs)
${}^3P_0 \to$						3.8
${}^1D_2$	2564	84.12	0.028	74.48	0.041	
${}^1G_4$	926	2288	0.8	1582	0.7	
${}^3F_4$	722	1.513×10^4	5.1	1.045×10^4	4.3	
${}^3F_2$	637	1.727×10^5	58.4	1.529×10^5	62.8	
${}^3H_6$	610	1.691×10^4	5.7	1.694×10^4	7.0	
${}^3H_4$	484	8.879×10^4	30.0	6.140×10^4	25.2	
${}^1D_2 \to$						38.5
${}^1G_4$	1483	3077	11.6	2982	11.6	
${}^3F_4$	1000	1.323×10^4	50.0	1.294×10^4	50.4	
${}^3F_3$	957	751.5	2.8	699.4	2.7	
${}^3F_2$	844	1783	6.7	1493	5.8	
${}^3H_6$	797	1263	4.8	1009	3.9	
${}^3H_5$	678	71.67	0.3	60.21	0.2	
${}^3H_4$	595	6292	23.8	6502	25.3	
${}^1G_4 \to$						460.4
${}^3F_4$	3279	66.51	3.1	65.28	3.0	
${}^3F_3$	2857	9.473	0.4	10.00	0.5	
${}^3F_2$	2041	8.281	0.4	6.829	0.3	
${}^3H_6$	1774	692.8	32.0	658.8	30.6	
${}^3H_5$	1296	1057	48.8	1086	50.5	
${}^3H_4$	1013	330.0	15.3	324.6	15.1	

TABLE 3 Spontaneous emission probabilities $A_{JJ'}$, fluorescence branching ratios β, and radiative lifetimes τ_{r} of Pr^{3+}:$PbWO_4$ crystal determined by the modified J–O theory when the ${}^3H_4 \to {}^3P_2$ transition is excluded

The spontaneous emission probabilities $A_{JJ'}\left(J \to J'\right)$, fluorescence branching ratios β, and radiative lifetimes τ_{r} of some principal fluorescence manifolds for Pr^{3+} ions in $PbWO_4$ crystal are listed in Table 3. In this table, the branching ratios and emission probabilities for σ and π polarizations are listed separately. For the ${}^3P_0 \to {}^3F_3$ and ${}^3P_0 \to {}^3H_5$ transitions, the values of $U^{(t)}$ ($t = 2, 4, 6$) are zero, so the corresponding data are not listed in the table.

3.4 *Fluorescence spectra*

Under excitation at 449 nm, the polarized fluorescence spectra of the sample were recorded in the spectral region 470–1080 nm at room temperature. Figure 2 shows that the π-polarized fluorescence is generally more intensive than the σ-polarized. In the π-polarized fluorescence spectrum, there are two peaks located at 489 and 648 nm with the same full width at half maximum (FWHM) of about 7.4 nm. In the σ-polarized fluorescence spectrum, the emission peaks are located at 491 nm and 648 nm with FWHMs of about 14.7 nm and 6.3 nm, respectively. It can also be seen from the figure that under excitation at 449 nm the emission transitions are mainly from the ${}^3P_0$ manifold, such as the intensive emissions from the ${}^3P_0 \to {}^3H_4$ and ${}^3P_0 \to {}^3F_2$ transitions around 489 and 648 nm, respectively, and some weak emissions related to other transitions from ${}^3P_j$ ($j = 0, 1, 2$) manifolds. However, the room-temperature fluorescence lines are too broad for precise assignment. Due to the low phonon energy of the $(WO_4)^{2-}$ group (about $900\,\mathrm{cm}^{-1}$) [4] and the large energy separation between the ${}^3P_0$ and ${}^1D_2$ manifolds (about $3608\,\mathrm{cm}^{-1}$), the multi-phonon relaxation from the ${}^3P_0$ manifold to the next-lower ${}^1D_2$ manifold is weak. The fluorescence branching ratios for the ${}^3P_0 \to {}^1D_2$ and ${}^3P_0 \to {}^1G_4$ transitions are also small (about 0.03% and 0.7%, respectively). So,

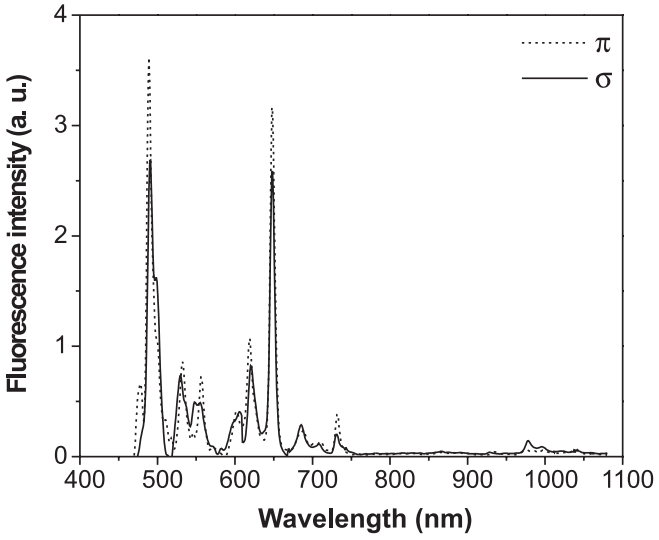

FIGURE 2 Room-temperature polarized fluorescence spectra of Pr^{3+}: $PbWO_4$ crystal under excitation at 449 nm

the fluorescence emissions from the $^1D_2$ and $^1G_4$ manifolds can hardly be observed in Fig. 2.

The room-temperature polarized fluorescence spectra in the spectral region 620–1500 nm of this crystal under $^1D_2$ excitation at 590 nm are shown in Fig. 3. Due to the absence of an appropriate filter, the fluorescence emission from the $^1D_2 \rightarrow {}^3H_4$ transition around 600 nm cannot be detected. Figure 3 shows that under $^1D_2$ excitation the fluorescence is dominated by the transitions from the $^1D_2$ manifold and the π-polarized fluorescence is generally more intensive than the σ-polarized. There are two main emission bands located around 900 nm and 1050 nm, corresponding to the $^1D_2 \rightarrow {}^3F_2$ and $^1D_2 \rightarrow {}^3F_4$ transitions in both σ- and π-polarized spectra. Weak fluorescence emission centered at 1336 nm and corresponding to the $^1G_4 \rightarrow {}^3H_5$ transition is observed because the $^1G_4$ manifold can be populated by the $^1D_2 \rightarrow {}^1G_4$ transition and because of a nearly resonant cross-relaxation process $(^1D_2, {}^3H_4) \rightarrow (^1G_4, {}^3F_4)$, which will be discussed in Sect. 3.5.

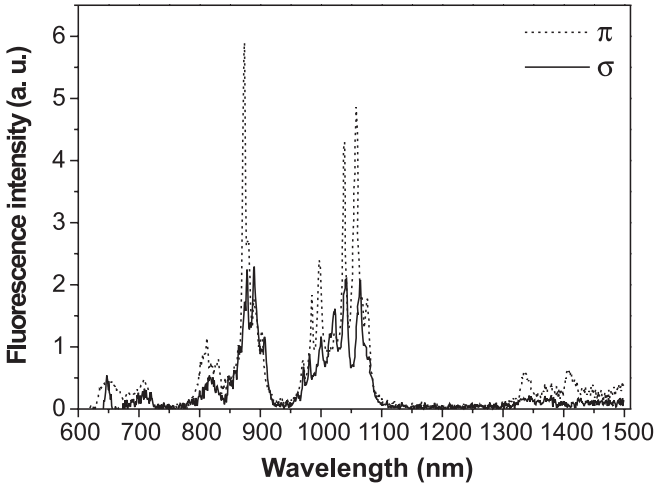

FIGURE 3 Room-temperature polarized fluorescence spectra of Pr^{3+} :$PbWO_4$ crystal under excitation at 590 nm

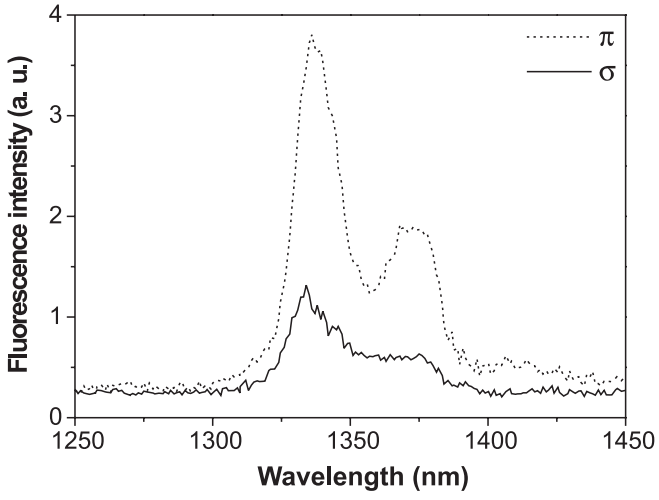

FIGURE 4 Room-temperature polarized fluorescence spectra of Pr^{3+}: $PbWO_4$ crystal under excitation at 1030 nm

Figure 4 shows the room-temperature polarized fluorescence spectra in the region of 1250–1450 nm under $^1G_4$ excitation at 1030 nm. Due to the low power of the Xe lamp used as excitation source at 1030 nm and the very weak absorption of the $^1G_4$ manifold, the signal-to-noise ratios of the spectra are quite low. The spectra are related to the $^1G_4 \rightarrow {}^3H_5$ transition. The fluorescence peaks and FWHMs of both σ- and π-polarized spectra are about 1336 nm and 50 nm, respectively, and the π-polarized fluorescence is also more intensive than the σ-polarized.

3.5 *Fluorescence lifetimes*

The fluorescence decay curve of the $^3P_0 \rightarrow {}^3H_4$ transition at the wavelength of 490 nm is shown in Fig. 5 in semilog scale. The linear relationship in the figure displays a single-exponential behavior of the fluorescence decay and the fluorescence lifetime of the $^3P_0$ manifold can be obtained

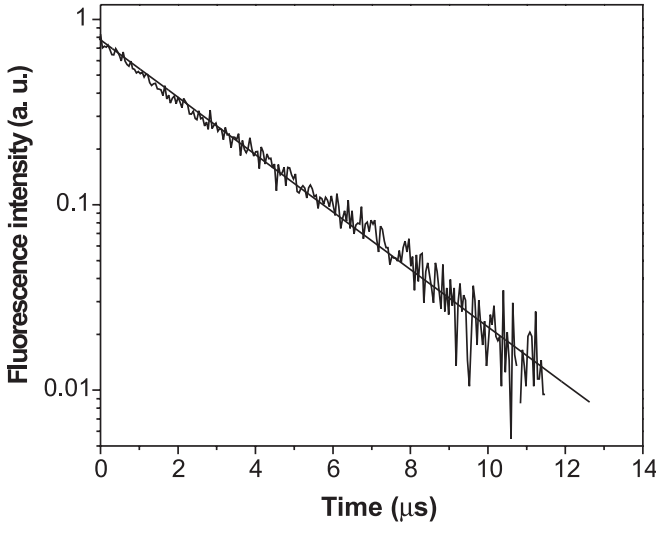

FIGURE 5 Room-temperature fluorescence decay curve at 490 nm of Pr^{3+}:$PbWO_4$ crystal under excitation at 449 nm. The fitting result of single-exponential decay is 2.8 μs

from the slope of the fitting line k, i.e. $\tau_f = -1/(2.303k)$. By fitting linearly, the slope is -0.1548, so the fluorescence lifetime of the $^3P_0$ manifold in Pr^{3+}:$PbWO_4$ crystal is about 2.8 μs. Then, the fluorescence quantum efficiency $\eta = \tau_f/\tau_r$ can be derived as 74%, which is comparable to 91% for Pr^{3+} in $Sr_5(PO_4)_3F$ [30] and higher than those of other Pr^{3+}-doped oxide crystals [22–24, 31]. The main reasons for the high quantum efficiency of Pr^{3+}:$PbWO_4$ crystal are the small phonon energy of the $(WO_4)^{2-}$ group (about 900 cm^{-1} [4]) in the crystal and the low Pr^{3+} concentration in the sample, which make the multi-phonon relaxation and the concentration quenching, respectively, weak.

When the Pr^{3+} ions were directly excited to the $^1D_2$ manifold at 590 nm, the fluorescence decay curve of the $^1D_2 \rightarrow {}^3H_5$ transition was measured at 706 nm. Different from that of the $^3P_0 \rightarrow {}^3H_4$ transition, the curve shown in Fig. 6 is not a single exponential at room temperature. It implies that the fluorescence emission from the $^1D_2$ manifold of Pr^{3+} in $PbWO_4$ crystal is strongly influenced by a nearly resonant cross-relaxation process involving the $^1G_4$ and $^3F_4$ manifolds $(^1D_2, {}^3H_4) \rightarrow (^1G_4, {}^3F_4)$. The process has also been observed in other Pr^{3+}-doped crystals [22, 23, 31, 32]. The non-exponential character of the fluorescence decay curve of the $^1D_2$ manifold can be analyzed using the continuum model proposed by Inokuti and Hirayama [33], who assumed energy transfer from an excited Pr^{3+} donor to the continuously distributed surrounding Pr^{3+} acceptors in the ground state. The fluorescence intensity can be expressed as

$$I(t) = I(0)\exp\left[-\frac{t}{\tau_0} - \Gamma\left(1-\frac{3}{s}\right)\frac{N_0}{C_0}\left(\frac{t}{\tau_0}\right)^{3/s}\right], \qquad (12)$$

where $I(t)$ is the fluorescence intensity at the time t, τ_0 is the fluorescence lifetime in absence of the energy transfer, N_0 is the Pr^{3+} concentration expressed in ion/cm^3, $C_0 = 3/4\pi R_c^3$ is the critical concentration related to the critical distance R_c defined as the distance at which the rate of energy transfer between the acceptor–donor pairs equals the spontaneous decay rate of the excited donor, $\Gamma(x)$ is the gamma function of x, and $s = 6, 8$, and 10 correspond to electric dipole–dipole, dipole–quadrupole, and quadrupole–quadrupole energy-transfer mechanisms, respectively.

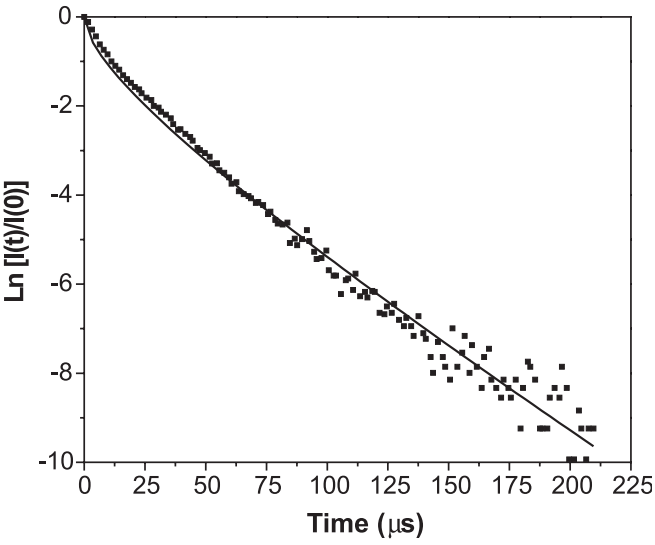

FIGURE 6 Room-temperature fluorescence decay curve at 706 nm corresponding to the $^1D_2 \rightarrow {}^3H_5$ transition of Pr^{3+}:$PbWO_4$ crystal under excitation at 590 nm. The *points* represent the experimental data and the *solid curve* is the fitting results based on the Inokuti–Hirayama model with $s = 6$

In Fig. 7 the fluorescence decay curve of the $^1D_2 \rightarrow {}^3H_5$ transition is plotted as $\ln[I(t)/I(0)] + t/\tau_0$ against $(t/\tau_0)^{3/s}$ and linear fitting based on the Inokuti–Hirayama model can be made to get the best value of s. Considering that the radiative lifetime τ_r obtained from the above J–O analysis does not include the non-radiative transitions caused mainly by multi-phonon relaxation and the fluorescence lifetime of a dilute

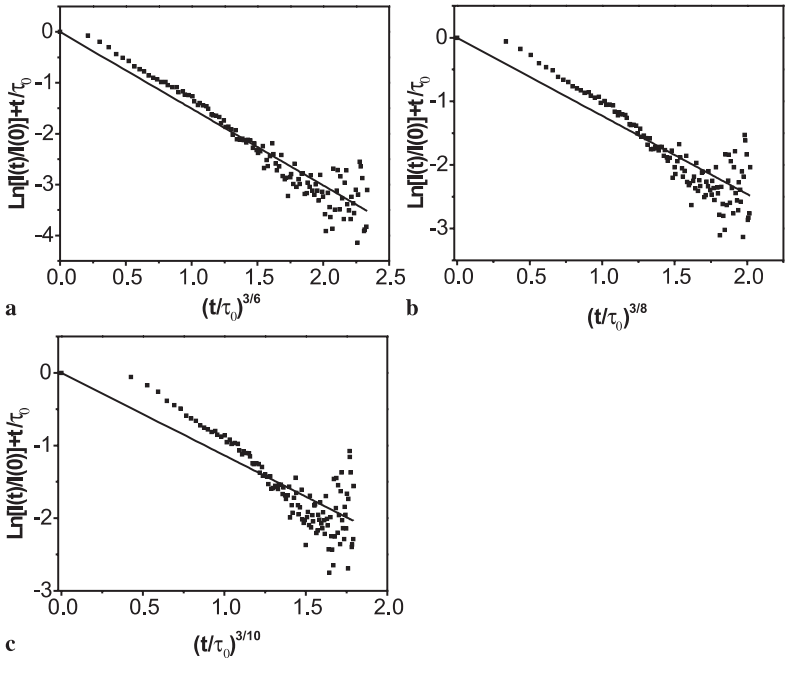

FIGURE 7 Inokuti–Hirayama presentations with **a** $s = 6$, **b** $s = 8$, and **c** $s = 10$ of the room-temperature fluorescence decay curve for the $^1D_2 \rightarrow {}^3H_5$ transition of Pr^{3+}:$PbWO_4$ crystal at 706 nm. The *points* represent the experimental results by plotting $\ln[I(t)/I(0)] + t/\tau_0$ against $(t/\tau_0)^{3/s}$ and the *solid lines* represent the Inokuti–Hirayama presentations

sample does not include the fluorescence quenching caused by Pr^{3+} concentration, either of them is not exactly the fluorescence lifetime τ_0 in absence of energy transfer at the practical Pr^{3+} concentration. Therefore, different from [17, 24, 32], τ_0, as well as C_0, was also treated as a variable parameter in the fitting process. Figure 7a–c show the fitting results of $s = 6$, 8, and 10, respectively, and the experimental curve had the best fitting with (12) when $s = 6$, corresponding to an electric dipole–dipole transfer mechanism. From the fitting, the fluorescence lifetime τ_0 in absence of energy transfer for 1.53 at. % Pr^{3+}-doped $PbWO_4$ crystal is obtained as 35.2 μs, which is close to the radiative lifetime τ_r of the $^1D_2$ manifold obtained from the modified J–O theory (about 38.5 μs). The reason is that the multi-phonon relaxation from the $^1D_2$ manifold to the next-lower manifold $^1G_4$ is relatively weak in tungstate crystal due to the low phonon energy of the $(WO_4)^{2-}$ group and the large separation between them.

As shown in Fig. 6, the good agreement of the fitting demonstrates that the cross-relaxation energy transfer caused by the electric dipole–dipole transfer mechanism is responsible for the non-exponential character of the fluorescence decay from the $^1D_2$ manifold for Pr^{3+} ions in $PbWO_4$. From the fitting, the critical concentration $C_0 = 3/4\pi R_c^3$ is derived as $1.96 \times 10^{20}\,cm^{-3}$ and the critical distance R_c is 1.07 nm. The average Pr–Pr distance in the crystal can be obtained from $R_{avg} = (4\pi N_0/3)^{-1/3}$ and $R_{avg} = 1.13$ nm, where N_0 is the Pr^{3+} concentration expressed in ion/cm^3. Because the average distance R_{avg} is close to the critical distance R_c, it is very probable to find an acceptor (Pr^{3+} ion in ground state) inside the critical distance of a donor (Pr^{3+} ion in excited state) and the cross-relaxation energy transfer is significant. The short R_c also indicates that the concentration-dependent fluorescence quenching may be strong for the $^1D_2$ manifold in Pr^{3+}:$PbWO_4$ crystal [17, 24].

Transition	Peak wavelength (nm)	Polarization	FWHM (nm)	σ_e^α (10^{-19} cm^2)
$^3P_0 \rightarrow {}^3H_4$	491	σ	14.7	0.71
$^3P_0 \rightarrow {}^3H_4$	489	π	7.4	1.15
$^3P_0 \rightarrow {}^3H_6$	620	σ	10.5	0.59
$^3P_0 \rightarrow {}^3H_6$	619	π	7.4	0.63
$^3P_0 \rightarrow {}^3F_2$	648	σ	6.3	9.18
$^3P_0 \rightarrow {}^3F_2$	648	π	7.4	10.23
$^3P_0 \rightarrow {}^3F_4$	731	σ	7.4	0.66
$^3P_0 \rightarrow {}^3F_4$	731	π	6.3	1.68

TABLE 4 Spectroscopic parameters of emissions from the $^3P_0$ manifold of Pr^{3+}:$PbWO_4$ crystal

3.6 *Stimulated emission cross section*

The stimulated emission cross section can be estimated from the room-temperature fluorescence spectrum according to [34]

$$\sigma_e^\alpha = \frac{\lambda^5 \beta}{8\pi c n^2 \tau_r} \frac{3I^\alpha(\lambda)}{\int [2I^\sigma(\lambda) + I^\pi(\lambda)]\,\lambda\,d\lambda}, \quad (13)$$

where α is the σ or π polarization and $I(\lambda)$ is the fluorescence intensity at wavelength λ. Due to the higher quantum efficiency of the $^3P_0$ manifold, especially the far more resistance to concentration quenching than the $^1D_2$ manifold [22], the potential application of Pr^{3+}:$PbWO_4$ as laser crystal is mainly related to the emission from the $^3P_0$ manifold. The peak emission wavelengths and cross sections, and the FWHMs of emission bands corresponding to the transitions from the manifold, are summarized in Table 4. It is worth noting that the peak emission cross sections of the $^3P_0 \rightarrow {}^3F_2$ red laser channel are 9.18×10^{-19} cm^2 (σ) and 10.23×10^{-19} cm^2 (π), which are approximately 4.9 times larger than that of Pr^{3+}-doped $LiYF_4$ crystal, in which a red laser has been realized [35, 36].

In Table 5, the main spectroscopic parameters related to the $^3P_0$ manifold of some Pr^{3+}-doped crystals are compared. It reveals that the Pr^{3+}:$PbWO_4$ crystal is comparable to other Pr^{3+}-doped oxide and fluoride crystals in spectral properties, so the Pr^{3+}:$PbWO_4$ crystal is a good candidate as a medium for solid-state lasers.

4 Conclusions

Polarized absorption spectra, polarized fluorescence spectra, and fluorescence decay curves of Pr^{3+} in $PbWO_4$ crystal were measured at room temperature. The polarized absorption spectra were analyzed by the standard J–O theory and the modified J–O theory proposed by Dunina et al. [27], and the best fitting results were obtained by the modified J–O theory without the $^3H_4 \rightarrow {}^3P_2$

Crystal	Ω_t (10^{-20} cm^2)			N_0 (at. %)	$^3P_0$ manifold			σ_e (10^{-19} cm^2)			Ref.
	$t=2$	$t=4$	$t=6$		τ_r (μs)	τ_f (μs)	η (%)	$^3P_0 \rightarrow {}^3H_4$	$^3P_0 \rightarrow {}^3H_6$	$^3P_0 \rightarrow {}^3F_2$	
$PbWO_4$	19.76	5.57	7.30	1.53	3.8	2.8	74	1.15 (E//c) 0.71 (E⊥c)	0.63 (E//c) 0.59 (E⊥c)	10.23 (E//c) 9.18 (E⊥c)	This work
$Mg:SrAl_{12}O_{19}$	0.84	2.19	6.86	1	38	61	63	1.05 (E⊥c)	0.30 (E//c) 0.39 (E⊥c)	0.61 (E⊥c)	[22]
$KGd(WO_4)_2$	19.50	7.31	4.86	0.1	5.8	0.06	1	-	-	-	[24]
$Sr_5(PO_4)_3F$	1.18	2.99	1.82	1	116	105	91	-	-	0.42	[30]
$Ca_3Sc_2Ge_3O_{12}$	2.92	1.69	1.86	7.2	37	14	38	0.73	1.24	1.02	[31]
$LiYF_4$	0.00	8.07	7.32	1.2	-	36	-	~1.9 (E//c) ~0.2 (E⊥c)	~1.3 (E//c) ~1.3 (E⊥c)	~2.1 (E//c) ~0.3 (E⊥c)	[35, 36]
$YAlO_3$	2.00	6.00	7.00	1	-	8.8	-	-	2.6 (E//a) 6.4 (E//b) 5.1 (E//c)	1.5 (E//a)	[20, 37]

TABLE 5 Comparison of spectroscopic parameters of Pr^{3+}-doped crystals (a *dash* indicates that the datum is not currently available)

transition. The three effective J–O parameters were obtained: $\Omega_2^{\text{eff}} = 19.76 \times 10^{-20}\,\text{cm}^2$, $\Omega_4^{\text{eff}} = 5.57 \times 10^{-20}\,\text{cm}^2$, and $\Omega_6^{\text{eff}} = 7.30 \times 10^{-20}\,\text{cm}^2$. The stimulated emission cross sections of the transitions from the $^3P_0$ manifold were determined. The radiative lifetimes of some typical fluorescence manifolds, including $^3P_0$, $^1D_2$, and $^1G_4$ manifolds, are derived as 3.8 μs, 38.5 μs, and 460.4 μs, respectively. The room-temperature fluorescence lifetime and quantum efficiency of the $^3P_0$ manifold are 2.8 μs and 74%, respectively.

The non-exponential character of the fluorescence decay curve of the $^1D_2$ manifold can be attributed to a nearly resonant cross-relaxation energy transfer involving the $^1G_4$ and $^3F_4$ manifolds. In fitting the fluorescence decay curve of the $^1D_2$ manifold based on the Inokuti–Hirayama model, the fluorescence lifetime τ_0 in absence of energy transfer is treated as a variable parameter and derived as 35.2 μs.

Results of this work demonstrate that the Pr^{3+}-doped $PbWO_4$ crystal has good spectroscopic and laser properties and is a potential candidate for solid state laser materials. The $^3P_0$ manifold of the Pr^{3+}-doped $PbWO_4$ crystal is more suitable as the upper laser level than the $^1D_2$ manifold. Furthermore, it has been found that the largest Raman gain is achieved when $PbWO_4$ crystal is excited by a laser with polarization parallel to the c axis of the crystal, but no Raman conversion is observed when the pump polarization is perpendicular to the c axis [2]. For the Pr^{3+}:$PbWO_4$ crystal, it is shown that both the absorption and the emission cross sections of the π-polarized spectrum are larger than those of the σ-polarized spectrum. Therefore, the Pr^{3+}:$PbWO_4$ crystal may also be an efficient self-stimulated Raman laser crystal in the visible region.

ACKNOWLEDGEMENTS We would like to thank Prof. Xiqi Feng (Shanghai Institute of Ceramics, Chinese Academy of Sciences) for providing the Pr^{3+}:$PbWO_4$ crystal. This work has been supported by the National Natural Science Foundation of China (Grant No. 50372068) and the Major Programs of Science and Technology Foundation of Fujian Province (Grant Nos. 2002H004 and 2004HZ01-1).

REFERENCES

1 M. Kobayashi, Y. Usuki, M. Ishii, T. Yazawa, K. Hara, M. Tanaka, M. Nikl, K. Nitsch: Nucl. Instrum. Methods A **399**, 261 (1997)
2 A.A. Kaminskii, C.L. McCray, H.R. Lee, S.W. Lee, D.A. Temple, T.H. Chyba, W.D. Marsh, J.C. Barnes, A.N. Annanenkov, V.D. Legun, H.J. Eichler, G.M.A. Gad, K. Ueda: Opt. Commun. **183**, 277 (2000)
3 Y. Huang, X. Feng, Zh. Xu, G. Zhao, G. Huang, Sh. Li: Solid State Commun. **127**, 1 (2003)
4 A.A. Kaminskii, H.J. Eichier, K. Ueda, N.V. Klassen, B.S. Redkin, L.E. Li, J. Findeisen, D. Jaque, J. Garcia-Sole, J. Fernandez, R. Balda: Appl. Opt. **38**, 4533 (1999)
5 W. Chen, Y. Inagawa, T. Omatsu, M. Tateda, N. Takeuchi, Y. Usuki: Opt. Commun. **194**, 401 (2001)
6 D.R. Simons, A.J. Faber, H. Dewaal: Opt. Lett. **20**, 468 (1995)
7 E. van der Kolk, P. Dorenbos, C.W.E. van Eijk: Opt. Commun. **197**, 317 (2001)
8 E. Osiac, E. Heumann, G. Huber, S. Kuck, E. Sani, A. Toncelli, M. Tonelli: Appl. Phys. Lett. **82**, 3832 (2003)
9 S. Nicolas, E. Descroix, M.F. Joubert, Y. Guyot, M. Laroche, R. Moncorge, R.Y. Abdulsabirov, A.K. Naumov, V.V. Semashko, A.M. Tkachuk, M. Malinowski: Opt. Mater. **22**, 139 (2003)
10 B.P. Singh, K.K. Sharma, J.S. Minhas: J. Phys. C: Solid State Phys. **19**, 6655 (1986)
11 M. Nikl, P. Bohacek, E. Mihokova, N. Solovieva, M. Martini, A. Vedda, P. Fabeni, G.P. Pazzi, M. Kobayashi, M. Ishii, Y. Usuki, D. Zimmerman: J. Cryst. Growth. **229**, 312 (2001)
12 K.D. Chang, H.J. Lee, H.S. Jang, K.S. Choi, S.Y. Lee, S.D. Choi: J. Appl. Phys. **91**, 2766 (2002)
13 Yu.A. Hizhnyi, S.G. Nedilko: J. Luminesc. **102–103**, 688 (2003)
14 B.R. Judd: Phys. Rev. **127**, 750 (1962)
15 G.S. Ofelt: J. Chem. Phys. **37**, 511 (1962)
16 S. Baccaro, L.M. Barone, B. Borgia, F. Castelli, F. Cavallari, I. Dafinei, F. de Notaristefani, M. Diemoz, A. Festinesi, E. Leonardi, E. Longo, M. Montecchi, G. Organtini: Nucl. Instrum. Methods A **385**, 209 (1997)
17 A. Mendez-Blas, M. Rico, V. Volkov, C. Cascales, C. Zaldo, C. Coya, A. Kling, L.C. Alves: J. Phys.: Condens. Matter **16**, 2139 (2004)
18 W.F. Krupke: Phys. Rev. **145**, 325 (1966)
19 A.A. Kaminskii: *Laser Crystals, their Physics and Properties* (Springer, Berlin 1981)
20 A.A. Kaminskii: *Crystalline Lasers: Physical Processes and Operating Schemes* (CRC, New York 1996)
21 M.J. Weber, B.H. Matsinger, V.L. Donlan, G.T. Surratt: J. Chem. Phys. **57**, 562 (1972)
22 L.D. Merkle, B. Zandi, R. Moncorge, Y. Guyot, H.R. Verdun, B. McIntosh: J. Appl. Phys. **79**, 1849 (1996)
23 A. Brenier, I.V. Kityk: J. Appl. Phys. **90**, 232 (2001)
24 C. Zaldo, M. Rico, C. Cascale, M.C. Pujol, J. Massons, M. Aguilo, F. Diza, P. Porcher: J. Phys.: Condens. Matter **1**, 8531 (2000)
25 J.A.M. Neto, D.W. Hewak, H. Tate: J. Non-Cryst. Solids **183**, 201 (1995)
26 R.S. Quimby, W.J. Miniscalco: J. Appl. Phys. **75**, 613 (1994)
27 E.B. Dunina, A.A. Kaminskii, A.A. Kornienko, K. Kurbanov, K.K. Pukhov: Sov. Phys. Solid State **32**, 290 (1990)
28 P. Goldner, F. Auzel: J. Appl. Phys. **79**, 7972 (1996)
29 Z. Luo, X. Chen, T. Zhao: Opt. Commun. **134**, 415 (1997)
30 D.K. Sardar, F. Castano: J. Appl. Phys. **91**, 911 (2002)
31 S. Pinelli, S. Bigotta, A. Toncelli, M. Tonelli, E. Cavalli, E. Bovero: Opt. Mater. **25**, 91 (2004)
32 B. Savoini, J.E.M. Santiuste, R. Gonzalez: Phys. Rev. B **56**, 5856 (1997)
33 M. Inokuti, F. Hirayama: J. Chem. Phys. **43**, 1978 (1965)
34 B.F. Aull, H.P. Jenssen: IEEE. J. Quantum Electron. **QE-18**, 925 (1982)
35 T. Sandrock, T. Danger, E. Heumann, G. Huber, B.H.T. Chai: Appl. Phys. B **58**, 149 (1994)
36 D.S. Knowles, Z. Zhang, D. Gabbe, H.P. Jenssen: IEEE J. Quantum Electron. **QE-24**, 1118 (1988)
37 T. Danger, A. Bleckmann, G. Huber: Appl. Phys. B **58**, 413 (1994)